LAWRENCE
LIVERMORE
NATIONAL
LABORATORY

LLNL-JRNL-646593

Light-powered bioelectronic devices with biologically-tunable performance

R. Tunuguntla, M. Bangar, K. Kim, P. Stroeve, C. Grigoropoulos, C. Ajo-Franklin, A. Noy

November 20, 2013

Advanced Materials

Disclaimer

Light-powered bioelectronic devices with biologically-tunable performance

R. Tunuguntla,[1,2] M. Bangar,[1,4,†] K. Kim,[1,6,†] P. Stroeve,[2] C. P. Grigoropoulos,[6] C. M. Ajo-Franklin,[4,5] A. Noy[1,3,*]

[1] *Biology and Biotechnology Division, Physical and Life Sciences Directorate, Lawrence Livermore National Laboratory, Livermore, CA 94550 USA*
[2] *Chemical Engineering Department, University of California Davis, Davis, CA 95340 USA*
[3] *School of Natural Sciences, University of California Merced, Merced, CA 95340 USA*
[4] *The Molecular Foundry, Materials Sciences Division and [5]Physical Biosciences Division, Lawrence Berkeley National Laboratory, Berkeley, CA 94720 USA*
[6] *Mechanical Engineering Department, University of California Berkeley, Berkeley, CA 94704 USA*

[†] *These authors contributed equally to this work*

[*] *E-mail: noy1@llnl.gov*

ABSTRACT

Many key biological processes ranging from cell signaling to energy production involve active and passive ion translocation across cell membranes and often other proteins and small molecule mediators provide critical regulation of such transport. Here we adapted these biological regulation mechanisms to control bioelectronic devices based on silicon nanowire transistors that incorporate a functional light-activated proton pump, bacteriorhodopsin (bR). bR acts as a biological gate that allows the device to convert protein photocycle events into a transistor response. Co-assembly of several different ionophores in the device allowed us to regulate two key parameters that determine the device functionality: the proton accumulation and proton gradient relief rates. These results demonstrate that biological regulation mechanisms can be used to tune bioelectronic device performance.

Biological systems interact with their environments by creating ion gradients, membrane electric potentials, or proton motive force to accomplish strikingly complex tasks on the nanometer length scale, such as energy harvesting, and whole organism replication. Most of this activity involves a vast arsenal of active and passive ion channels, membrane receptors and ion pumps that mediate complex and precise transport across

biological membranes[1]. Despite the remarkable rate of progress exhibited by modern microelectronic devices, they still cannot compete with efficiency, precision, and flexibility of biological systems on the component level. On the flipside, the sophistication of these molecular machines provides an excellent opportunity to use them in hybrid bioelectronic devices where such a combination could deliver enhanced electronic functionality and seamless bi-directional interfaces between man-made and biological structures[2].

One-dimensional inorganic nanostructures, which have critical dimensions comparable to the sizes of biological molecules, form an excellent materials platform for building such integrated assemblies. Researchers already use silicon nanowire (SiNW) field effect transistors functionalized with molecular recognition sites in biosensing[3, 4, 5], nucleic acid detection[4], and drug development[6] applications. Recent works achieved an even higher level of integration by interfacing these transistor devices to neuronal activity[7], and cyborg tissue scaffolds[8]. We have been developing a platform for integration of membrane protein functionality into electronic devices based on a 1D lipid bilayer device architecture. In these devices, the membrane proteins reside within the lipid bilayer that covers a nanowire channel of a SiNW field-effect transistor. This lipid bilayer performs several functions: it shields the nanowire from the solution species and serves as a native-like environment for membrane proteins that preserves their functionality, integrity, and even vectorality. In the past, we showed that this architecture allows us to couple passive ion transport[9] and active ATP-driven ion transport to the electronic signaling[10].

In this work, we show a 1-D bilayer device incorporating a bR proton pump that couples light-driven proton transport to a bioelectronic circuit output. Significantly, these devices also use a distinct biological mechanism for regulating their performance where co-

assembly of protein channels and ionophores in the 1-D bilayer results in the modified device output levels and response times.

Device design and operation. Our basic device platform (**Fig. 1a**) was based on a microfabricated SiNW field-effect transistor in which the nanowire ends were clamped between a pair of source and drain electrodes insulated from the solution by a protective photoresist layer. A microfluidic channel filled with a buffer solution covered the active area of the chip. This configuration allowed us to fuse proteoliposomes to create a continuous lipid bilayer onto the SiNW surface while keeping the bilayer and proteins in their native hydrated state during subsequent device measurement. The lipid bilayer covering the nanowire surface contained bR, a protein from the purple membrane of *Halobacterium salinarum*. bR absorbs green light (λ_{max} = 560nm) and undergoes a multi-state photo-cycle that translocates a proton across the membrane[11]. In bacteria, this process builds up the proton motive force[12] that subsequently powers ATP synthesis. Bacteriorhodopsin is also exceptionally stable *ex-vivo* under diverse environmental stresses, and over a broad range of pH and temperature[13, 14].

After we reconstituted bR into preformed 1,2-Dioleoyl-sn-glycero-3-phosphocholine (DOPC) liposomes and fused these proteoliposomes onto the device surface, fluorescence microscopy imaging (**Fig. 1b**) indicated that the lipid bilayer covered the nanowire device completely. Moreover, fluorescence recovery after photobleaching (FRAP) measurements indicated that the lipid bilayer covering the nanowire was continuous and mobile (Supplementary Fig. S2), both of which are important properties for providing good shielding of the SiNW surface and accommodateing the membrane proteins.

Upon exposure to the 530 nm green light, the SiNW devices that did not contain membrane proteins registered small amounts of photo-induced current (**Fig 1c**, black trace)[15]. This signal was quite small (the maximum conductance change was less than 0.1%) and exhibited almost instantaneous turn-on and turn-off kinetics: upon illumination the signal immediately increased to a steady-state level, which then decayed back to baseline level as soon as the light was turned off. When the lipid membrane covering the SiNW contained bR protein, the device showed a markedly different response to the green light exposure (**Fig 1c,** red trace). The source-drain current started to decrease with the magnitude of this decrease exceeding that of the photocurrent by at least an order of magnitude. Unlike the photocurrent signal, this signal change was not instantaneous, but instead showed a fast initial rate of change followed by gradual slow-down. After the illumination was switched off, the current slowly returned to its original level. This cycle was repeatable (**Fig. 1c**) without any significant losses of signal strength or fidelity. These observations indicate that the observed electronic response is caused by the photoinduced activity of bR protein.

We propose the following mechanism for the observed device response. It is unlikely that the proton gradient build-up and the associated electrical potential across the membrane are responsible for the slow-down, since this hypothesis cannot explain why the devices return to their initial state after the light is switched off. Instead, a much more likely mechanism involves the interplay of the two processes that occur in the illuminated device. Upon exposure to green light, the bR proteins in the lipid membrane start pumping protons across the lipid bilayer, building up a proton gradient across the bilayer. The resulting change in the SiNW surface charge due to the protonation of $SiOH^-$ groups causes

a decrease in the current output[16]. A competing process involves passive diffusion of protons across the lipid bilayer that tries to equilibrate the proton concentration on both sides of the membrane. The rate of diffusion increases with the increasing proton gradient magnitude, and the proton pumping rate does not. As these processes begin to cancel each other, the device rate of response slows down and eventually should reach a steady state. When the light is switched off and the protein stops pumping protons, the leakage through the bilayer continues to deplete the transmembrane proton gradient. Eventually the device returns to its baseline state and becomes ready to repeat this sequence of events during the next illumination cycle.

Quantitative Analysis of the Device Performance. The quantitative model, describing such kinetics is similar to the model of the operation of the Na,K-ATPase driven bioelectronic transistor[10]. The proton pumping and proton leakage rates define the two main model parameters. As long as the incident light intensity is not causing the protein response to saturate, the proton gradient build-up could be described as the zero-order process governed by the light-intensity-dependent rate of proton pumping, I_0. Proton leakage though the lipid bilayer obeys the Fick's law where the leakage rate, governed by the time, τ, is proportional to the magnitude of the transmembrane proton gradient. If we assume that the conductance shift of the device is proportional to the change in the proton concentration, C, (i.e. that the device operates within the linear part of the pH response curve of the SiNW transistor, Supplementary Fig. S4), then the kinetics of the device response can be described by a master equation:

$$\frac{dC}{dt} = I_0 - \frac{1}{\tau}\Delta C \qquad (1)$$

where $1/\tau$ represents a first-order kinetic constant for the leakage process. When the device is illuminated, then the proton concentration gradient should rise as:

$$C(t) = C_0 + I_0\tau\left(1 - e^{-\frac{t}{\tau}}\right) \qquad (2)$$

and when the light is switched off, the decay of the proton gradient can be described by:

$$\Delta C(t) = \Delta C_0 \cdot e^{-\frac{t}{\tau}} \qquad (3)$$

where ΔC_0 is the proton gradient value reached at the moment when the device was shut off. Indeed, the device response kinetics follow the relationships predicted by the Eq. 2,3 (**Fig. 2a**).

This model also points to several key features of the device kinetics. First, as the proton leakage process plays a role both during the light-ON and light-OFF cycles, the leakage time estimated from the rise and fall regions of the response curve should be identical, which is indeed what we observed in the experiments (**Fig. 2a**, inset). Second, the initial pumping rate should show the linear dependence on the intensity of the incident light, at least until bR activity reaches saturation. Again, the values of the initial pumping rates that we measured at 5 different light intensities follow this dependence (**Fig. 2b**).

Biological modulation of the device operational characteristics. The dynamic equilibrium between the pumping and leakage processes that defines the device performance also gives us an opportunity to vary the two key operational parameters—the protein pumping and the proton leakage rates. Previous studies of bR in cellular environments[17, 18, 19] found that proton-electrochemical gradient, $\Delta\mu_{H^+}$, across the membrane can influence bR's pumping efficiency[17]. Thus we can modify the device performance using different ionophore molecules that allow specific ions to cross the lipid

membrane. Three different ionophores that self-insert into the bilayer allowed us to vary different components of the proton-electrochemical gradient independently. Valinomycin, a hydrophobic carrier molecule that shuttles K^+ ions across the membrane in the direction of the electrochemical gradient [20, 21], relieves the electric field gradient across the membrane but leaves the proton gradient intact. Nigericin, a transmembrane carrier that catalyzes an electro-neutral K^+/H^+ exchange across the lipid bilayer [22, 23], relieves the proton gradient, but preserves the electric field gradient. Finally, gramicidin A (gramA), a peptide that forms a passive channel in the membrane allowing fast ion leakage[24], neutralizes both of these gradients.

Valinomycin, which allows only K^+ ions to cross the membrane, provides an effective compensatory pathway to relieve the electrical potential across the bilayer while keeping the proton gradient intact. Since this activity relieves the back-pressure caused by the electrochemical gradient, on the proton pump, we expect that bR protein should be able to develop a larger pH gradient under the bilayer in presence of valinomycin. Indeed, addition of 2 μM of valinomycin to the 1-D bilayer device increased the peak proton accumulation under the bilayer surface by ~50% (decreasing the pH by additional 0.3 units) compared to devices containing only bR (**Fig. 3a**). This effect was also repeatable over multiple light on/off cycles. The initial pumping rate also increased almost 2-fold compared to devices containing bR only (**Fig. 4a).** The origin os this effect is best understood by considering that the maximum proton gradient that can be generated in the device is given by the value of the proton concentration when the proton flux generated by the pump is equal to the proton flux leaking through the bilayer:

$$\Delta C_{max} = I_0 \cdot \tau \qquad (4)$$

According to Eq. 4, increased protein pumping rate should lead to the enhanced device response. Another confirmation of this mechanism comes from the values for the proton leakage rate time constant: as we expected, valinomycin addition did not significantly change the proton leakage rate (**Fig. 4c**).

Incorporation of nigericin, an electro-neutral antiporter ionophore, exploits a different aspect of our device functionality. Nigericin facilitates the back-flux of the protons pumped under the bilayer by bR, thus providing some relief for the proton gradient. Since this action is accompanied by the coupled flux of potassium ions in the opposite direction, this ionophore preserves the electrical field gradient developed by bacteriorhodopsin. By providing an extra leakage pathway for the protons, nigericin effectively reduces the efficiency of the proton pumping; therefore, according to Eq. 4, the maximum signal achieved by the device should also be reduced relative to the signal obtained before introduction of the ionophore. Indeed, the experiment shows (**Fig. 3b**) that after addition of 2 μM of nigericin the maximum proton accumulation was decreased by 35% (a ΔpH difference of 0.2 units) compared to devices with only bR proteins. In this instance, we see that the initial pumping rate decreased approximately 2-fold at the maximum light intensity (**Fig. 4b**). Additionally, since nigericin provides another leakage pathway for protons, we saw a faster leakage time, τ, during the light-ON state (**Fig. 4c**).

Finally, we explored a way to drastically increase the proton leakage rate though the lipid bilayer by introducing gramA to our devices. GramA is a passive pore that exhibits high permeability for protons and monovalent ions. The presence of GramA pores in the bilayer-coated device effectively shorts the lipid membrane and provides a major pathway to relive all ion and proton gradients in the system[25, 26]. Indeed, when we introduced a

GramA to our devices, most of the proton pump activity got suppressed and we observe only very small SiNW conductance change in response to the green light illumination (**Fig. 3c**).

In this work, we used hierarchical assembly of membrane protein pumps and ionophore molecules to create biologically-tunable bioelectronic devices that converted light-induced proton transport by bacteriorhodopsin protein into an electronic signal. Our results show that addition of ionophores to the system can tune the device output by altering the two dominant kinetic processes in the system: proton pumping by the bR protein, and passive proton leakage through the lipid bilayer. Furthermore, different ionophores were able to modulate different system parameters. Valinomycin enhanced the initial device response rate, and increased the overall level of device response. Nigericin, in contrast, reduced the overall device response and the initial device response rate. Co-reconstitution of gramA into the lipid membrane abolished the device response and effectively neutralized the pH gradient buildup by perforating the lipid bilayer.

These results open up new opportunities for constructing new types of bioelectronic devices. The incorporation of a robust proton pump capable of developing significant pH gradients is a major step towards integration of other biological processes powered by proton gradients to nanoelectronic circuits. Most significantly, the possibility to tune the device performance by using biological modifiers co-assembled in the membrane covering the nanowire gives researchers a much more extensive biological toolkit for bioelectronics applications.

Methods

SiNW growth and FET device fabrication. P-type silicon nanowires with diameters in the range of 40-80 nm were grown using catalytic chemical vapor deposition (CVD). SiNWs were aligned onto a SiO_2 surface using flow alignment technique[27]. A source-drain electrode contacts with a typical spacing of 5 μm were patterned on the wafer using photolithography, and the chip was subsequently passivated with an additional photoresist layer, creating a 2 μm channel exposing the SiNWs. Devices were subsequently placed into a PDMS fluid cell with inlet/outlet ports for solution delivery, and an opening for a leak-free gate electrode (see details in Supplementary Information).

Proteoliposome preparation and characterization. 1,2-Dioleoyl-sn-glycero-3-phosphocholine (DOPC) proteoliposomes were prepared using the detergent mediated reconstitution method[28] in 150 mM KCl, 1 mM KH_2PO_4, pH 6.8 at a protein: lipid molar ratio of 1:500. Successful incorporation of bR (Sigma-Aldrich) into liposomes was verified using UV-Vis spectroscopy and dynamic light scattering (DLS) measurements before and after reconstitution. The PDMS channel was filled with 150 mM KCl, 1 mM KH_2PO_4, pH 6.8 buffer solution.

Confocal laser scanning microscopy. Lipid bilayer coverage and mobility on the SiNW were verified by adding a small amount of TexasRed-DHPE to the lipid mixture and imaging the bilayer with a scanning confocal microscope (Zeiss LSM710 with Zen software). Further experimental details are provided in the Supplementary Information.

Device Measurements. Assembled devices were mounted in a shielded probe station. Transfer characteristics (I_{S-D} vs V_G) and real time (I_{S-D} vs t) measurements were recorded with a home-built measurement system that used a NI-DAQ card and a Keithley 428-PROG pre-amplifier. To improve the signal to noise ratio we have applied an AC bias between the

source and drain electrodes and used lock-in detection to measure the source-drain current. For device photoactivation we used an external LED light source (SCHOTT KL 2500) fitted with a green (560 nm) bandpass filter (Newport Corp.). The light source output had a power density of 136 mW/cm^2 at 100% illumination and a spot size of 1 cm in diameter.

Ionophore Incorporation. Ionophores, valinomycin and nigericin, were added to the solution in the PDMS microfluidic channel at a final concentration of 2 μM and incubated in the fluid cell for approximately 30 min to allow sufficient time for incorporation into the bR containing bilayer. Afterwards, the chamber was washed with buffer. GramA was co-reconstituted with bR during proteoliposome preparation, at a ratio of 1:200 gramA: lipid.

Acknowledgements

This work was supported by the U.S. Department of Energy, Office of Basic Energy Sciences, Division of Materials Sciences and Engineering. Work at the Lawrence Livermore National Laboratory was performed under the auspices of the U.S. Department of Energy under Contract DE-AC52-07NA27344. Work at the Molecular Foundry was supported by the Office of Science, Office of Basic Energy Sciences, of the U.S. Department of Energy under Contract No. DE-AC02-05CH11231. R.T. acknowledges support from the LSP program at LLNL.

Author Contributions:

AN conceived and directed research; RT, MB, KK and CAF developed the sample preparation and characterization protocols; RT, MB, and KK set up the measurement hardware and performed the measurements; MB and KK developed the fabrication

procedure; RT, MB, and AN analyzed the data; all authors participated in discussing research and writing the manuscript.

References

1. Alberts B, Bray D, Lewis J, Raff M, Roberts K, Watson JD. *Molecular Biology of the Cell*, 5 edn. Garland Science: New York, 2007.

2. Noy A. Bionanoelectronics. *Adv Mater.* 2011, **23**(7)**:** 799-799.

3. He B, Morrow TJ, Keating CD. Nanowire sensors for multiplexed detection of biomolecules. *Curr Opin Chem Biol* 2008, **12**(5)**:** 522-528.

4. Gao A, Lu N, Wang Y, Dai P, Li T, Gao X*, et al.* Enhanced Sensing of Nucleic Acids with Silicon Nanowire Field Effect Transistor Biosensors. *Nano Letters* 2012, **12**(10)**:** 5262-5268.

5. Lin S-P, Pan C-Y, Tseng K-C, Lin M-C, Chen C-D, Tsai C-C*, et al.* A reversible surface functionalized nanowire transistor to study protein–protein interactions. *Nano Today* 2009, **4**(3)**:** 235-243.

6. Duan X, Li Y, Rajan NK, Routenberg DA, Modis Y, Reed MA. Quantification of the affinities and kinetics of protein interactions using silicon nanowire biosensors. *Nat Nano* 2012, **7**(6)**:** 401-407.

7. Patolsky F, Timko BP, Yu G, Fang Y, Greytak AB, Zheng G*, et al.* Detection, Stimulation, and Inhibition of Neuronal Signals with High-Density Nanowire Transistor Arrays. *Science* 2006, **313**(5790)**:** 1100-1104.

8. Bozhi Tian, Jia Liu, Tal Dvir, Lihua Jin, Jonathan H. Tsui, Quan Qing*, et al.* Macroporous nanowire nanoelectronic scaffolds for synthetic tissues. *Nat Mater* 2012, **11:** 986–994.

9. Misra N, Martinez JA, Huang S-C, Wang Y, Stroeve P, Grigoropoulos C*, et al.* Bioelectronic Silicon Nanowire Devices Utilizing Functional Membrane Proteins. *Proc Natl Acad Sci USA* 2009, **106**(33)**:** 13780–13784 .

10. Huang S-C, Artyukhin A, Misra N, Martinez J, Stroeve P, Grigoropoulos C*, et al.* Carbon nanotube devices controlled by an ion pump. *Nano Lett* 2010, **10**(5)**:** 1812–1816.

11. Royant A, Edman K, Ursby T, Pebay-Peyroula E, Landau EM, Neutze R. Helix deformation is coupled to vectorial proton transport in the photocycle of bacteriorhodopsin. *Nature* 2000, **406**(6796)**:** 645-648.

12. Lozier RH, Bogomolni RA, Stoeckenius W. Bacteriorhodopsin: a light-driven proton pump in Halobacterium Halobium. *Biophys J* 1975, **15**(9)**:** 955–962.

13. Thavasi V, Lazarova T, Filipek S, Kolinski M, Querol E, Kumar A*, et al.* Study on the Feasibility of Bacteriorhodopsin as Bio-Photosensitizer in Excitonic Solar Cell: A First Report. *J. Nanosci. Nanotech.* 2009, **9**(3)**:** 1679-1687.

14. Quan R, Ya-Pu Z, Li H, Hui-Bin Z. A nanomechanical device based on light-driven proton pumps. *Nanotechnol.* 2006, **17**(6)**:** 1778.

15. Kim K-HK, Kihyun; Jeong, Dong-Young; Min, Byungdon; Cho, Kyoungah; Kim, Hyunsuk; Moon, Byung-Moo; Noh, Taeyong; Park, Jucheol; Suh, Minchul; Kim, Sangsig Photocurrent of Undoped, n- and p-Type Si Nanowires Synthesized by Thermal Chemical Vapor Deposition. *Jpn J Appl Phys* 2006, **45**(5A)**:** 4265-4269.

16. Cui Y, Wei Q, Park H, Lieber CM. Nanowire Nanosensors for Highly Sensitive and Selective Detection of Biological and Chemical Species. *Science* 2001, **293**(5533)**:** 1289-1292.

17. Joshi MK, Bose S, Hendler RW. Regulation of the Bacteriorhodopsin Photocycle and Proton Pumping in Whole Cells of Halobacterium salinarium. *Biochemistry* 1999, **38**(27)**:** 8786-8793.

18. Sherman WV, Caplan SR. Arrhenius parameters of phototransients in Halobacterium halobium in physiological conditions. *Nature* 1975, **258**(5537)**:** 766-768.

19. S L Helgerson MKM, D B Bivin, P K Wolber, E Heinz, and W Stoeckenius. Coupling between the bacteriorhodopsin photocycle and the protonmotive force in Halobacterium halobium cell envelope vesicles. III. Time-resolved increase in the transmembrane electric potential and modeling of the associated ion fluxes. *Biophys J* 1985 **48**(5)**:** 709–719.

20. Garlid KD, Paucek P. Mitochondrial potassium transport: the K+ cycle. *Biochimica et Biophysica Acta (BBA) - Bioenergetics* 2003, **1606**(1–3)**:** 23-41.

21. Johnson SM, Bangham AD. Potassium permeability of single compartment liposomes with and without valinomycin. *Biochim Biophys Acta - Biomembranes* 1969, **193**(1)**:** 82-91.

22. Rigaud JL, Bluzat A, Buschlen S. Incorporation of bacteriorhodopsin into large unilamellar liposomes by reverse phase evaporation. *Biochem Bioph Res Co* 1983, **111**(2)**:** 373-382.

23. Hellingwerf KJ, Arents JC, Scholte BJ, Westerhoff HV. Bacteriorhodopsin in liposomes. II. Experimental evidence in support of a theoretical model. *Biochim Biophys Acta - Bioenergetics* 1979, **547**(3)**:** 561-582.

24. Kelkar DA, Chattopadhyay A. The gramicidin ion channel: A model membrane protein. *Biochim Biophys Acta - Biomembranes* 2007, **1768**(9)**:** 2011-2025.

25. Clement NR, Gould JM. Kinetics for the development of gramicidin-induced ion permeability in unilamellar phospholipid vesicles. *Biochemistry* 1981, **20**(6)**:** 1544-1548.

26. Prabhananda BS, Kombrabail MH. Two mechanisms of H+/OH- transport across phospholipid vesicular membrane facilitated by gramicidin A. *Biophys J* 1996, **71**(6)**:** 3091-3097.

27. Huang Y, Duan X, Wei Q, Lieber CM. Directed Assembly of One-Dimensional Nanostructures into Functional Networks. *Science* 2001, **291**(5504)**:** 630-633.

28. Paternostre MT, Roux M, Rigaud JL. Mechanisms of membrane protein insertion into liposomes during reconstitution procedures involving the use of detergents. 1. Solubilization of large unilamellar liposomes (prepared by reverse-phase evaporation) by Triton X-100, octyl glucoside, and sodium cholate. *Biochemistry* 1988, **27**(8)**:** 2668-2677.

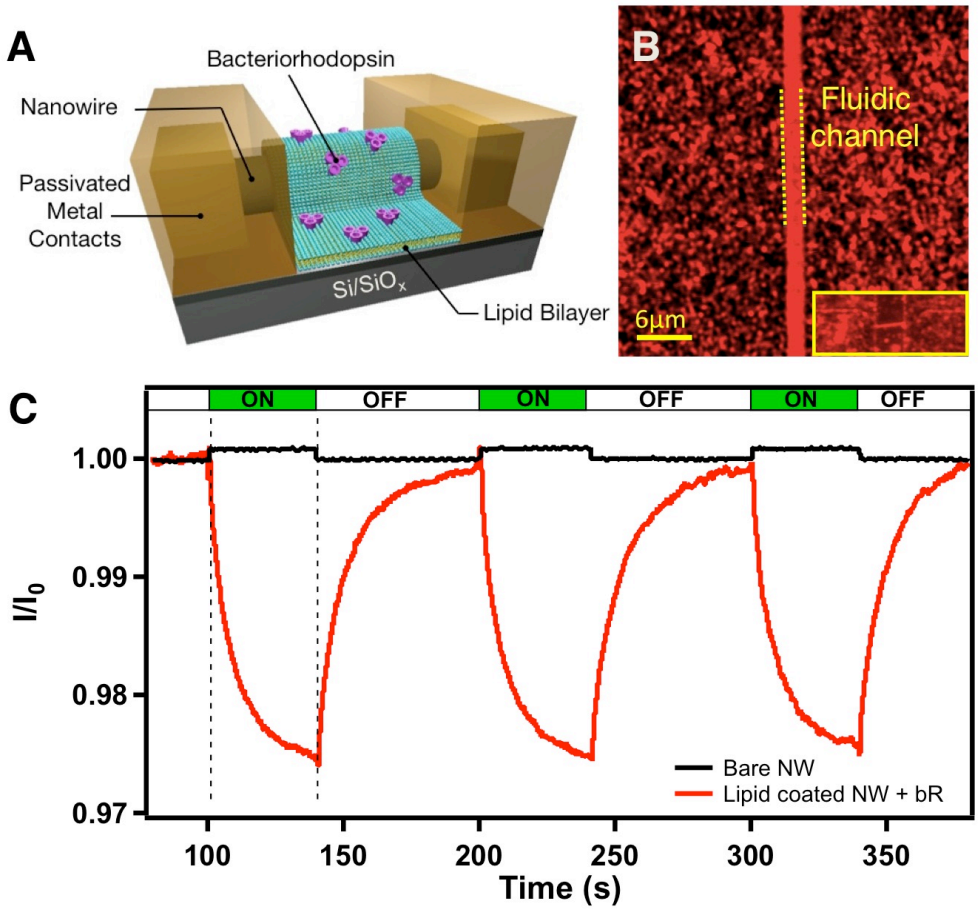

Figure 1. **Light-activated bioelectronic device.** **A**. Device schematics showing a SiNW transistor with the nanowire covered with a lipid bilayer containing bacteriorhodopsin protein. **B**. Scanning confocal microscopy image of the chip coated with lipid bilayer. To visualize the bilayer a small portion of the lipid was labeled with a TexasRed™ fluorescent dye. Inset: a scanning confocal microscope image of a single device region of the chip showing a SiNW covered with lipid bilayer. **C.** Normalized time trace of the SiNW transistor source-drain current recorded under 3 cycles of green light (530nm) illumination for the uncoated SiNW device (black trace) and the device coated with a lipid bilayer containing bR protein (red trace).

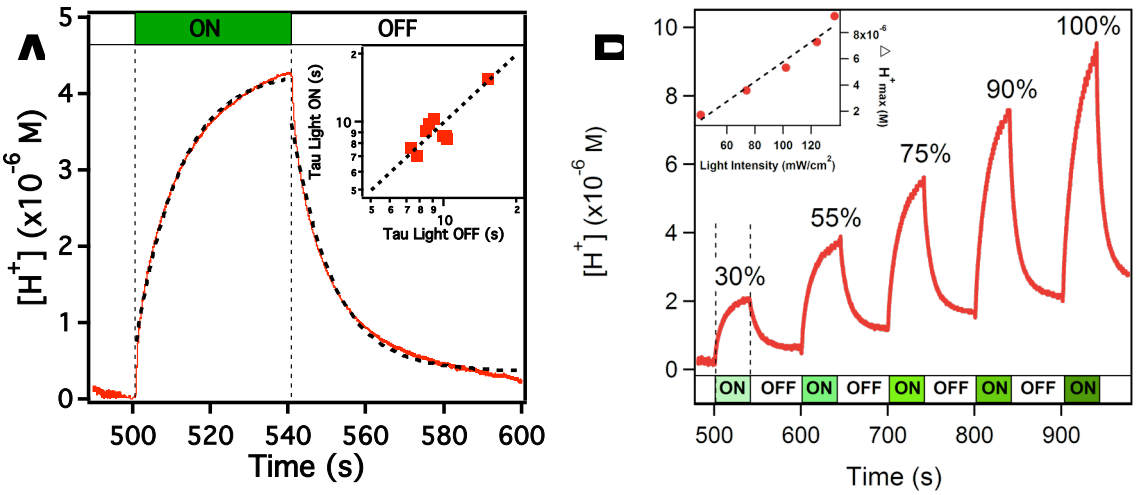

Figure 2. Kinetics of the device response. **A**. Time trace of the proton concentration in the space between the SiNW and the lipid bilayer over one light ON/light OFF cycle for the device incorporating bR proteins (each cycle consisted of 40s light exposure followed by 60s of dark time). Dashed lines represent the best fit to Eq. 2 and 3. **Inset**: A log-log plot of the proton leakage time values obtained from the fits. **B**. Time trace of the proton concentration next to the SiNW surface in another device under illumination cycles of different intensity. **Inset**: A plot of the maximum proton accumulation as a function of incident light intensity.

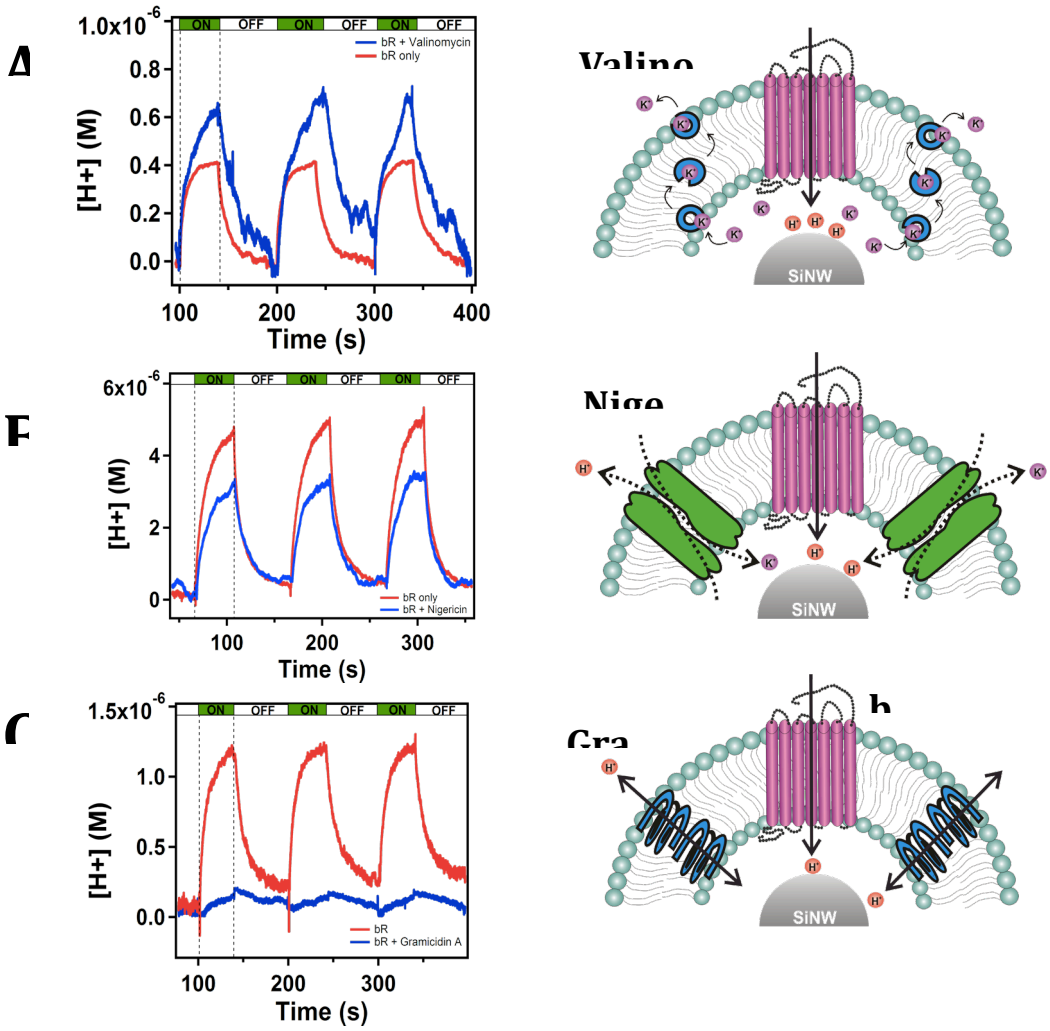

Figure 3. Device response in presence of ionophores. Time traces of the proton concentration in the space between the SiNW and the lipid bilayer for the devices incorporating bR proteins and (**A**) valinomycin, (**B**) nigericin, and (**C**) gramicidin A. Schematics on the right side illustrate the action mechanism for each ionophore.

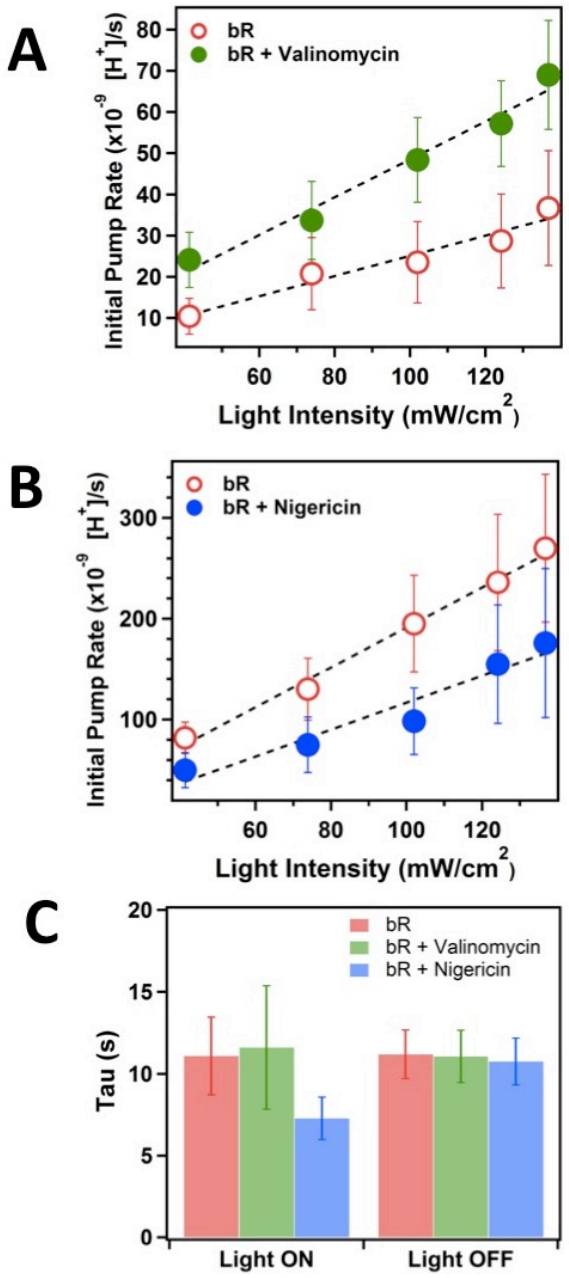

Figure 4. **Bioelectronic device performance in presence of ionophores.** (**A**). A plot comparing the initial bR pumping rate measured in the device incorporating bR protein before (empty red circles), and after (filled green circles) addition of 2 μM valinomycin. (**B**), A plot comparing the initial bR pump rates for bR containing devices before (empty red

circles) and after (blue filled circles) exposure to 2 μM nigericin. (C). Bar graph showing the values for the average proton leakage time through the lipid bilayer measured with the light ON and light OFF for devices containing bR only (red), bR and valinomycin (green), and bR and nigericin (red).

SUPPLEMENTARY INFORMATION FOR:

Light-powered bioelectronic devices with biologically-tunable performance

R. Tunuguntla,[1,2] M. Bangar,[1,4,†] K. Kim,[1,6,†] P. Stroeve,[2] C. P. Grigoropoulos,[6] C. M. Ajo-Franklin,[4,5] A. Noy[1,3,*]

[1] *Biology and Biotechnology Division, Physical and Life Sciences Directorate, Lawrence Livermore National Laboratory, Livermore, CA 94550 USA*
[2] *Chemical Engineering Department, University of California Davis, Davis, CA 95340 USA*
[3] *School of Natural Sciences, University of California Merced, Merced, CA 95340 USA*
[4] *The Molecular Foundry, Materials Sciences Division and [5]Physical Biosciences Division, Lawrence Berkeley National Laboratory, Berkeley, CA 94720 USA*
[6] *Mechanical Engineering Department, University of California Berkeley, Berkeley, CA 94704 USA*

† *These authors contributed equally to this work*

* *E-mail: noy1@llnl.gov*

1. DETAILED MATERIALS AND METHODS

1. 1. SI substrates

Heavily p-type doped (<0.005 Ω.cm) 4' silicon (100) wafers with 300 nm thermal oxide wafers from Silicon Quest International were used as the substrate for various synthesis and fabrication steps.

1. 2. CVD Synthesis of Silicon Nanowires (SiNWs)

Silicon wafers were diced into smaller pieces, cleaned with IPA, dried under N_2 stream. These Si pieces were then treated with 0.1% (weight/volume) aqueous solution of poly-L-lysine (PLL) for 5 min, rinsed with DI water, and dried under N_2 stream. A drop of 30 nm gold colloid catalyst solution (Ted Pella) was dispersed onto the chip, incubated for 60s and rinsed with DI water. Excess PLL was removed from the chip using O_2 plasma treatment at 50W for 5 min.

The growth substrate was then placed in a 1-inch tube furnace. Nanowire growth was carried out at a chamber pressure of 100 Torr and a temperature of ~480 ^{0}C using 36 sccm of SiH_4 gas (10% silane in Helium) as a Si precursor and 4 sccm of B_2H_6 (100ppm diborane in Helium) as dopant. 30-minute long growth

produces a large amount of nanowires in the 40 to 80 nm diameter range. To harvest the nanowires for subsequent device fabrication use, the chip with the grown nanowires was placed in 1mL of ethanol and sonicated in a water bath sonicator for 1-3 s.

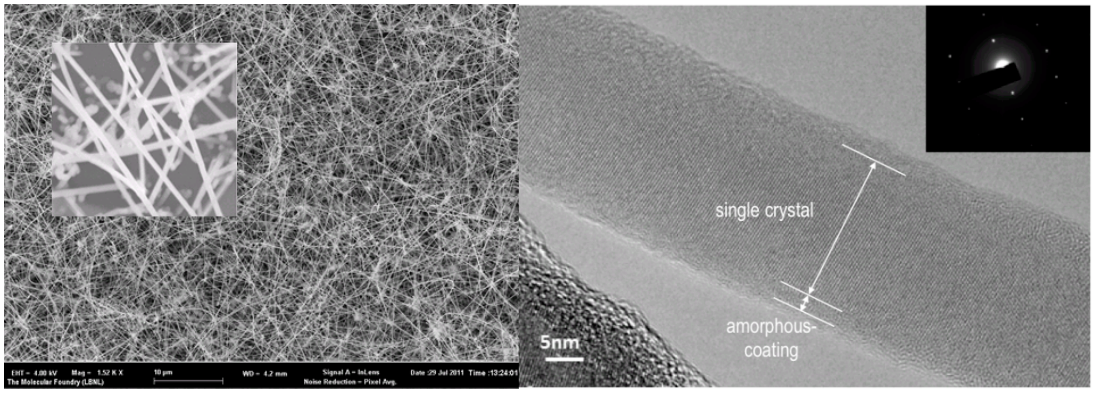

Supplemental Figure S1: [Left] SEM image of SiNW forest on the growth substrate. Inset shows magnified view of SiNWs with diameter in the range of 40-80 nm. [Right] TEM images of SiNW showing crystalline core with amorphous shell. Inset shows electron diffraction of the crystalline core indicating single crystal of Si.

1.3. PDMS Micro-channel fabrication

PDMS pre-polymer solution and the curing agent at a ratio of 10:1 (weight/weight) were thoroughly mixed and degassed using vacuum. PDMS was cast on a microchannel pattern [500 μm × 50 μm × 1 cm (w × h × l)] pre-patterned with SU8 photoresist on a silicon wafer and was cured at ~80 ^{0}C on a hotplate for 1hr. Micro-channels 'stamps' were cut from the master-mold and sonicated in ethanol for 5 min to clean them before use.

1.4. Silicon nanowire FET device fabrication

I. Nanowire alignment:

Silicon wafers were dehydrated in 180 ^{0}C convection oven for about 30 min and allowed to cool to room temperature. Subsequently, wafer was treated with 0.1% (weight/volume) aqueous solution of PLL for 3min rinsed with DI water and dried under N_2 stream. A PDMS micro-channel stamp was placed on the device silicon and nanowire suspension was flowed through the channel at 0.1 ml/min flow rate to deposit and align the nanowire in the direction of the flow. Alternatively, the

nanowires were deposited onto the wafer directly using the dry transfer method. In one variation a small chip with as-grown nanowires was translated across the wafer. In another, the nanowires were first deposited onto a PDMS stamp surface by touching the stamp to the nanowire chip and then touching the stamp to the wafer surface. PLL was subsequently removed using oxygen plasma etching as described in the previous sections. At the last step the wafer was annealed at 180 ^{0}C for 10min in inert gas.

II. Source-drain electrode patterning:

Device wafer with aligned nanowires was again dehydrated in 180 ^{0}C convection oven for about 30 min and allowed to cool to room temperature. LOR-3A photoresist was spun on the wafer at 4000 rpm for 40 s to obtain ~350 nm thick film. Wafer was baked at 180 ^{0}C for 5 min in a convection oven. After cooling the wafer to room temperature, S1805 photoresist was spun onto the wafer at 4000 rpm for 40 s to obtain film thickness of ~400 nm. Wafer was subsequently baked for 90 s at 110 °C on a hotplate.

The wafer chip was exposed through a photomask using an aligner tool (ABM Inc.) operated in a vacuum contact mode for ~3 s at 17 mW/cm^2. The exposed wafer was developed in AZ-300 MIF developer for 20-40 s using gentle agitation. Wafer was immediately washed with DI water and dried in N_2. Wafer was cleaned with O_2 plasma at 30 W to remove any residual photoresist from the developed regions.

Native oxide on the silicon nanowires in the open contact regions was etched away using buffered oxide etchant (BOE) for 7-8 s followed by rinsing with DI water and drying with N_2. 100 nm Ni was subsequently deposited, at a pressure below ~1×10^{-7} Torr, onto the patterned chip to define source and drain electrode contacts to the nanowire with 5 μm spacing. Lift-off was carried out in Remover-PG at 70 ^{0}C to define the final device structure.

III. Device Annealing:

After lift-off, device wafer was annealed at 380°C in a forming gas 10% H_2/90% N_2

for 2 min using a rapid thermal annealing apparatus to form ohmic contacts between the nanowire and the nickel contact electrodes. A pre-soak at 200˚C for 2 min was used to eliminate any moisture prior to carrying out the higher-temperature anneal.

IV. Electrode passivation:

Contact Ni electrodes were further passivated by spin coating the wafer with HMDS adhesion promoter at 1000 rpm for 40 s followed by spin-coating of photoresist S1805 at 4000 rpm for 40 s. Photoresist layer was further baked at 115 ^{0}C for 90 sec and patterned using a photomask on an optical aligner similar to earlier step. Mask was aligned to the metal contact electrode layer so that a 2 μm channel is exposed in the gap between metal contact electrodes. The pattern was developed in AZ 300-MIF developer to form the channel that exposes SiNWs in the region between metal electrodes.

For measurements the device chip was mounted in an in-house-built holder with a PDMS channel (similar to the one used for nanowire alignement) that had inlet/outlet opening for liquid flow and an opening for mounting a leak-free Ag/AgCl reference electrode (Warner Instruments, LLC) that was used as a gate electrode.

1.5. **Liposome and proteoliposome with Bacteriorhodopsin (bR) formation**

300 μl of DOPC (10 mg/ml) in chloroform (Avanti Polar Lipids) were added to a glass vial with a Teflon-lined lid. For fluorescence imaging 11 μl of TexasRed-DHPE lipid (10 mg/ml) in chloroform was added to the lipid composition. Chloroform was subsequently evaporated in a Biotage V-10 evaporator to form a lipid film on the vial walls. This vial was further stored in a vacuum desiccator overnight to ensure complete removal of chloroform before use. Dried lipid film was then hydrated with 1 ml of 150 mM KCl, 1 mM KH_2PO_4, pH 6.8 buffer to a final lipid concentration of 3 mg/ml and extruded through a 200nm pore size filter using a hand-extruder (Avanti Polar Lipids).

For bacteriorhodopsin incorporation into the liposomes, pre-formed vesicles were de-stabilized with n-dodecyl-β-D-maltoside (βDDM, Sigma-Aldrich). Purified

bacteriorhodopsin (Sigma-Aldrich, some bR protein was also provided by M. Coleman (LLNL)) was added to the de-stabilized vesicle solution to a final bR: lipid molar ratio of 1:500 and final βDDM concentration of 0.008%. This solution was incubated at room temperature for 45 mins and then the surfactant was slowly removed by using bio-bead SM-2 adsorbent (Bio-Rad). Stepwise addition and removal of 40 mg/mL bio-beads to the proteoliposome solution was done 5 times over 5 hours of incubation. This solution was further purified to remove unincorporated bR and any remaining surfactant micelles by size exclusion column chromatography using 10 mL columns (Pierce) packed with Sepharose CL-6B (Sigma-Aldrich). Fractions were collected and analyzed with Nanodrop 2000 UV-Vis (Thermo-Scientific) to identify the fraction containing bR proteoliposomes.

1.6. Gramicidin An (gramA) incorporation in the bR reconstituted vesicles

Gramicidin A was dissolved in ethanol to obtain a final concentration of 5mg/ml. 300 μl of DOPC was added to a glass vial with a Teflon-lined lid. An aliquot of the gramA solution was added to the same glass vial to obtain a mixture containing gramA: lipid at molar ratio of 1:200. Subsequently, the solution mixture was dried to form a film. Starting with this lipid/gramA film, proteoliposomes were prepared as described in the previous section.

1.7. Lipid Bilayer Fusion on Silicon Nanowire Devices

Liposome solutions were flown over the SiNW FET devices through the PDMS microfluidic channel and allowed to fuse over the nanowire surface for a minimum of 30 min, followed by washing with copious amounts of 150 mM KCl, 1 mM KH_2PO_4, pH 6.8 buffer, to remove un-ruptured vesicles. Bilayer formation, uniformity and mobility were evaluated by incorporating 0.5% Texas-Red-DHPE lipid (Invitrogen) into the lipid composition. To estimate the mobility of lipid molecules in the bilayer we performed fluorescence recovery after photobleaching (FRAP) experiments using a confocal microscope (Zeiss LSM 710).

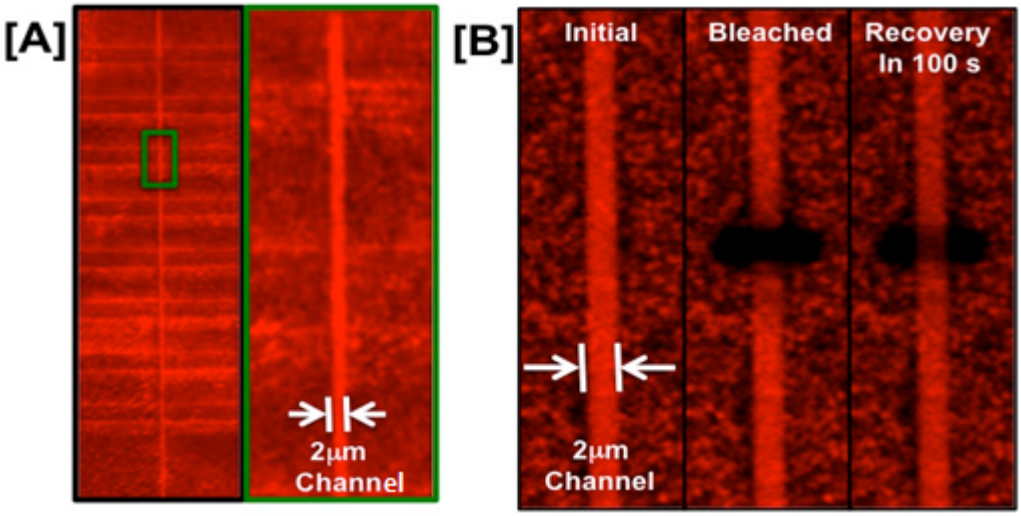

Supplemental Figure S2: [A] Texas red fluorescence images showing uniform bilayer coverage in the 2 μm active photoresist channel between metal contact electrode region on the device chip. [B] FRAP images show TR-DHPE fluorescence initially, after bleaching, and recovery after 100 s in the channel region. These images show uniform bilayer in the channel region. Bilayer mobility in the channel region was calculated to be ~1 $\mu m^2/s$.

2. SiNW TRANSISTOR CHARACTERIZATION

Fully assembled devices were mounted onto a probe station shielded with a Faraday cage. Transfer characteristic ($I_{S\text{-}D}$ vs V_G or *I-V*) and real time ($I_{S\text{-}D}$ vs t) measurements were done using a home-built measurement system that used a set of NI-DAQ cards (National Instruments) for AC source-voltage (V_S) application. Lock-in detection was performed using Keithley 428-PROG preamplifier along with National Instrument's lock-in kit for LabView. I-V curve acquisition and time-trace measurements were carried out using AC source-drain bias of 200 mV (amplitude) at 5 Hz and 100 Hz frequencies.

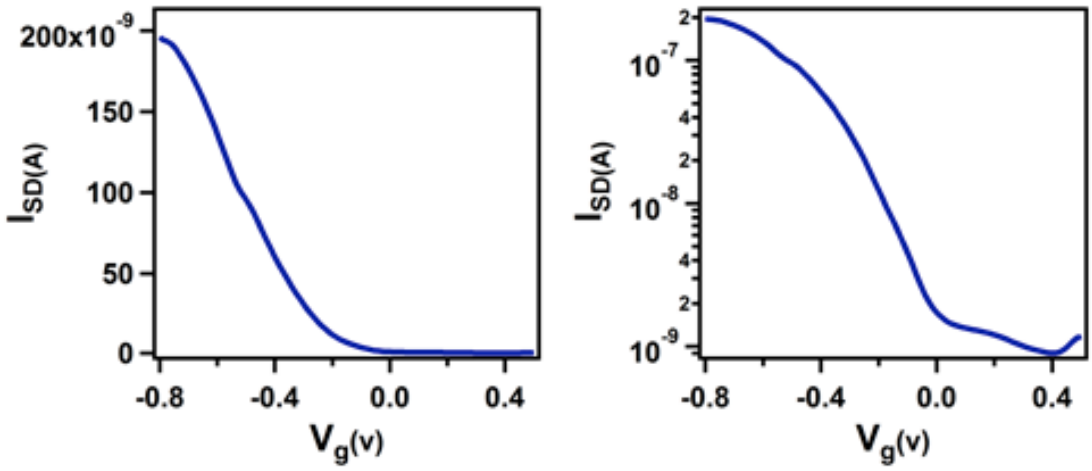

Supplemental Figure S3: Transfer characteristics for the bare SiNW FET device fabricated (right: linear scale, left: log scale) shows excellent device performance with on/off ration of ~10^3.

3. pH RESPONSE OF SiNW TRANSISTORS

We have obtained pH response of the bare SiNW devices by flowing buffer solution of different pH through the fluid cell and recording the steady-state conductance of the device. The pH response shows a well-defined transition centered around pH=5.4

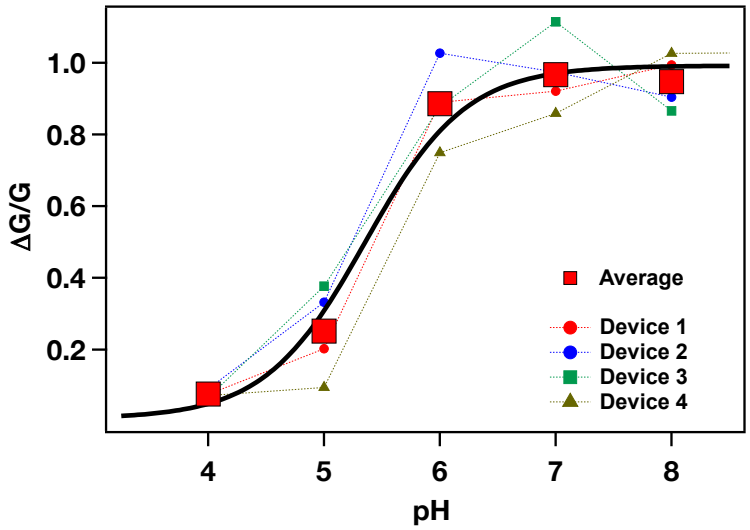

Supplemental Figure S4: Averaged pH response curve (red filled squares) and individual pH response curves (dotted lines) for 4 SiNW FET devices. Black solid line shows the fit of the averaged data to the Henderson-Hasselbalch equation with the fitted pKa value of 5.3558±0.196.